$e^+e^- \to b\bar b W^+W^-$ events at the Next Linear Collider: colour structure of top signal and irreducible background

17 October 1996

PHYSICS LETTERS B

ELSEVIER

Physics Letters B 387 (1996) 411–418

$b\bar{b}W^+W^-$ production at hadron colliders. Top signal and irreducible backgrounds ★

Alessandro Ballestrero, Ezio Maina, Marco Pizzio

Dipartimento di Fisica Teorica, Università di Torino, and INFN, Sezione di Torino, v. Giuria 1, 10125 Torino, Italy

Received 8 July 1996
Editor: R. Gatto

Abstract

We compute complete tree level matrix elements for $gg, q\bar{q} \to b\bar{b}W^+W^-$. We analyze the irreducible backgrounds to top signal at the Tevatron and at the LHC. Their contribution to the total cross section is about 5% at the LHC, due to single resonant channels. Several distributions with contributions from signal and backgrounds are presented.

1. Introduction

With the discovery of the top quark at the Tevatron [1] by the CDF and D0 Collaboration, all fermions belonging to the three generations which, according to the LEP measurement of the invisible width of the Z, possess a light neutrino have been observed.

Using 67 pb^{-1} of data CDF measured the top mass to be $M_t = 176 \pm 8(\text{stat}) \pm 10(\text{syst})$ GeV and the production cross section as $\sigma_{tt} = 6.8^{+3.6}_{-2.4}$ pb. The larger sample of top events which has been subsequently collected will soon allow a better determination of the parameters and properties of the newly discovered particle. Already at this year's winter conferences new preliminary results have been presented, based on about 110 pb^{-1} of data [2]. The most precise measurement of the top mass, extracted from the lepton plus three or more jets sample, is $M_t = 175.6 \pm 5.7(\text{stat}) \pm 7.1(\text{syst})$ GeV. The corresponding result for the production cross section is $\sigma_{tt} = 7.5^{+1.9}_{-1.6}$ pb.

The mass of the top is a fundamental parameter of the Standard Model and plays a crucial role in radiative corrections to electroweak observables. In fact bounds on the top mass can be obtained from a comparison of high precision measurements at LEP and SLC, together with information from neutrino scattering, with the best theoretical predictions. Within the Standard Model the top mass must lie in the range $M_t = 178 \pm 8^{+17}_{-20}$ GeV [3]. The agreement between this indirect determination of M_t with the value which is directly measured at Fermilab is a remarkable success of the model. Any improvement in the precision of the top mass measurement, particularly when the mass of the W boson will be measured to a precision of about 50 MeV at LEP 2, will further test the electroweak theory, significantly reducing the allowed range for the mass of the Higgs boson.

It is obvious that the discovery of the top is only the first step. All details of the production process and decay will have to be thoroughly examined. The measurement of the production cross section and of

★ Work supported in part by Ministero dell' Università e della Ricerca Scientifica.
e-mail: ballestrero@to.infn.it,maina@to.infn.it,pizzio@to.infn.it.

PII S0370-2693(96)01048-9

the distributions of different kinematic variables, like the p_T of the top, the angular distribution of the decay products or the characteristics of additional gluon jets, will challenge our understanding of perturbative QCD. The determination of the top decay channels will test whether the new heavy quark behaves as predicted by the Standard Model and might provide a window on new physics. These studies will be continued at Fermilab after the construction of the Main Injector and will be further refined at the Large Hadron Collider (LHC), where the cross section is much larger than at Tevatron energy and at the Next Linear Collider (NLC), in the clean environment of an e^+e^- machine.

In order to achieve a complete understanding of top production, a theoretical effort matching the advances on the experimental side is required. The production cross section has long been computed at next to leading order (NLO) in QCD [4]. More recently the contribution of soft gluons have been resummed to all order [5] using different techniques. In Ref. [6] the resummation procedure has been applied to the inclusive transverse momentum and rapidity distributions of the top. Several kinematic distributions have been computed at NLO in Ref. [7]. All these studies have treated the top quark as a stable particle, separating the production of a $\bar{t}t$ pair from the independent decay of the two heavy quarks, in the spirit of the so-called narrow width approximation (NWA).

The overall uncertainty in the calculation of the total cross section due to different choices of parton distribution functions and of renormalization and factorization scales is of the order of 20%. The difference between pure NLO calculations and calculations which also resum soft gluon effects is also of order 20% at the Tevatron and as large as a factor of two at the LHC. These uncertainties however affect in a similar way all the contributions to the total cross section, including irreducible backgrounds whose relevance remains to be assessed.

In this letter we examine the production of the $b\bar{b}W^+W^-$ final state at the Tevatron and at the LHC, taking into account the full set of tree level diagrams. Our approach allows us to study the effects of the finite width of the top and of the irreducible background to $\bar{t}t$ production, including their interference. Correlations between the decays of the two t-quarks are automatically included.

A few representative diagrams are shown in Figs. 1

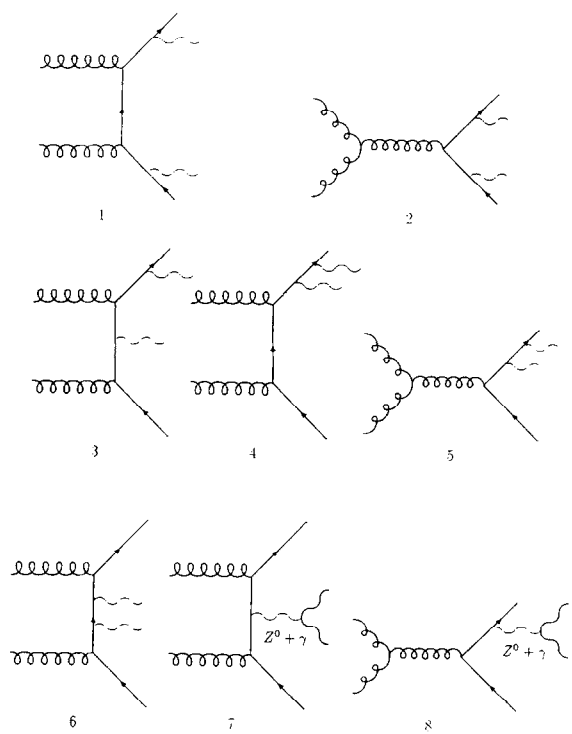

Fig. 1. Sample Feynman diagrams contributing in the lowest order to $gg \to b\bar{b}W^+W^-$. External wavy lines represent $W^\pm$ as appropriate. Internal wavy lines represent Z^0 and γ. Gluons permutation are not shown. In diagrams (3)-(5) only t-resonant diagrams are drawn; $\bar{t}$-resonant diagrams are obtained replacing $b \leftrightarrow \bar{b}$ and $W^+ \leftrightarrow W^-$. All other non-resonant diagrams can be obtained from (7), (8) changing the insertions of the internal vector boson lines (Z_0 and γ). SM Higgs contributions are not shown because their contribution is far below the accuracy reached in the present work. They can be obtained replacing internal neutral vector boson lines with scalar Higgs lines.

and 2. In addition to the standard mechanism which is $\mathcal{O}(\alpha^2\alpha_s^2)$ we have studied the contribution of the $\mathcal{O}(\alpha^4)$ diagrams in which an initial pair of light quarks annihilates to a photon or a Z boson. Many of the diagrams we are studying (3, 4, 5 in Fig. 1; 2 in Fig. 2), while contributing to the irreducible background to $t\bar{t}$ production, effectively represent the production of a *single* top and must be taken into account in any attempt to study this rarer top production mechanism which is of interest in his own right. The simpler process $q\bar{q} \to W^* \to tb$, for instance, has been discussed in Ref. [8] as a promising candidate for a precise measurement of the V_{tb} element of the CKM mixing matrix. In Ref. [9] the subset of diagrams (1,2 plus

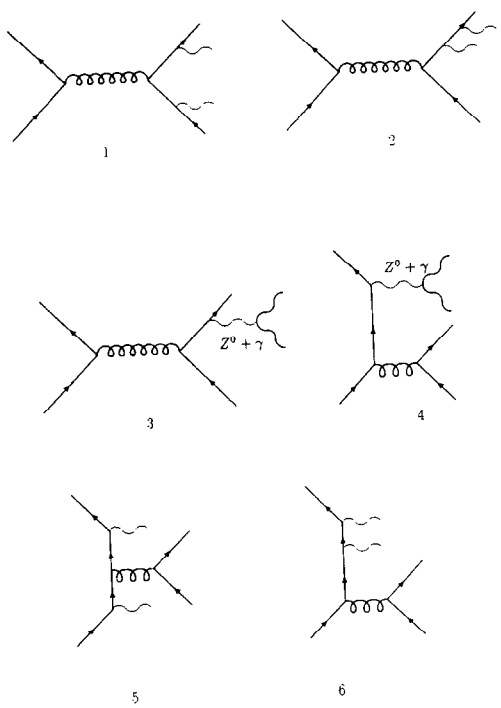

Fig. 2. Sample Feynman diagrams contributing in the lowest order to $q\bar{q} \to b\bar{b}W^+W^-$. External wavy lines represent $W^\pm$ as appropriate. Internal wavy lines represent Z^0 and γ. Gluons permutation are not shown. $\bar{t}$-resonant diagrams are obtained replacing $b \leftrightarrow \bar{b}$ and $W^+ \leftrightarrow W^-$ in diagram (2). All other non-resonant diagrams can be obtained from (3)-(6) changing the insertions of the internal vector boson lines (Z_0 and γ). SM Higgs contributions are not shown because their contribution is far below the accuracy reached in the present work. They can be obtained replacing internal neutral vector boson lines with scalar Higgs lines.

crossed in Fig. 1 and 1 in Fig. 2) which describe the production of a $\bar{t}t$ pair $\bar{q}q$, $gg \to \bar{t}t$ followed by the two decays $t \to W^+b$, $\bar{t} \to W^-\bar{b}$ has been studied using helicity amplitude methods. Strictly speaking, since the three diagrams discussed in Ref. [9] are not by themselves gauge invariant, the results obtained in this fashion are doubtful. It can however be argued that using an appropriate gauge, and under experimental conditions optimized for the observation of on-shell top pairs, the error will be of order Γ_t/M_t. Here we extend the helicity amplitude approach to the full gauge invariant set of diagrams which are required to describe $b\bar{b}W^+W^-$ production.

Within the present range of experimentally allowed top mass values [1], the top lifetime is of the order of 10^{-23} sec and the top decays to bW^+ before hadronizing. As a consequence, there might be significant finite width and irreducible background effects at the percent level. Indeed we have previously found corrections of this order of magnitude in $e^+e^- \to b\bar{b}W^+W^-$ at the NLC [10]. It is therefore important to evaluate these effects and, when relevant, fully include them in the theoretical analysis. The determination of the top mass and of the production cross section are clearly influenced by irreducible backgrounds and one cannot rely on the NWA without checking the size of the corrections to this approximation. Furthermore, signal and background usually have different distributions in phase space and the spectra of some interesting kinematical observables may be more sensitive to these corrections than the total cross section. Alternatively, these differences may be useful for a more effective separation of the top signal from non-resonant backgrounds.

We have made no approximation concerning the mass of the b, taking it into full account both in phase space and into the computation of the matrix elements. The b mass also regulates the collinear singularities that would be present in some of the non-resonant diagrams, for instance diagram 3, 4, 6 and 7 in Fig. 1, if we had treated the b quark as massless.

2. Calculation

The matrix elements for $gg \to W^+W^-\bar{b}b$ and $q\bar{q} \to W^+W^-\bar{b}b$ have been computed using helicity amplitude methods. For the first process the method of Ref. [11] has been used. The amplitude for the second reaction has been computed with the method described in Ref. [12]. The expression of the corresponding Feynman diagrams has been generated with the help of PHACT (Program for Helicity Amplitude Calculations with Tau matrices) [13]. We have checked our results for gauge and BRST invariance [14].

The full set of diagrams has been divided into four subsets, which were named after the corresponding structure of resonant enhancements as double resonant, t single resonant, $\bar{t}$ single resonant, and non-resonant.

Some representative diagrams for $gg \to W^+W^-\bar{b}b$ are shown in Fig. 1. The full set includes 39 $\mathcal{O}(\alpha^2\alpha_s^2)$ diagrams including 8 diagrams with a virtual Higgs. These latter are suppressed by the small coupling of

the Higgs boson to the b and can be neglected. Diagrams 1 and 2 are double resonant. They correspond in narrow width approximation to the production and decay of a $t\bar{t}$ pair. Integrating over the whole phase space the amplitude squared obtained from just these two diagrams, one reproduces in NWA the cross section for $gg \to \bar{t}t$. The branching ratio of t ($\bar{t}$) to W^+b ($W^-\bar{b}$) is in fact one, as we take off-diagonal CKM matrix elements to be zero.

Diagrams 3, 4 and 5 are examples of diagrams which are single resonant in the t channel. They correspond in narrow width approximation to the production of a t-quark together with a $\bar{b}W^-$ pair followed by the decay $t \to bW^+$. All diagrams in the same class can be obtained permuting gluon lines and connecting the negatively charged W in all possible positions, while leaving the W^+ next to the outgoing fermion. The single resonant diagrams corresponding to the production of a $\bar{t}$ particle can be easily obtained in a similar way. The remaining diagrams in Fig. 1, numbered 6, 7 and 8, are examples of non resonant diagrams.

Selected diagrams describing $q\bar{q} \to W^+W^-\bar{b}b$ are shown in Fig. 2. The full set includes 16 $\mathcal{O}(\alpha^2\alpha_s^2)$ diagrams including 2 diagrams with a virtual Higgs and 62 $\mathcal{O}(\alpha^4)$ diagrams, of which 11 include a Higgs. In the former case the diagrams with a Higgs propagator are suppressed by the $Hb\bar{b}$ coupling. In the latter case the Higgs can be connected with a large coupling to the intermediate Z. However the contribution of these diagrams can be relevant only if the Higgs mass is larger than $2M_W$ and the Higgs propagator can go on mass-shell. To simplify our argument, we have neglected all diagrams which include a Higgs particle, limiting our discussion to the diagrams which survive in the limit of an infinitely heavy Higgs. In case a Higgs is discovered, the complete set of diagrams would have to be considered. For a similar discussion at the NLC see [10,15]. In analogy with the $gg \to W^+W^-\bar{b}b$ case, the full set of diagrams can be subdivided in a double resonant (1 of Fig. 2) subset, two single resonant subsets corresponding to t production (2 of Fig. 2) and $\bar{t}$ production and a non-resonant subset (3, 4, 5, 6).

We have found it convenient to separate the different contributions to the cross section and to integrate them separately, adapting the choice of phase space variables to the peaking structure which correspond to the different sets of intermediate particles which can go on mass shell. We have identified a double resonant contribution generated by the modulus square of the corresponding diagrams and two single resonant contributions which include the modulus square of the single resonant diagrams plus the interference between single and double resonant diagrams. All remaining terms, the modulus square of non-resonant diagrams plus the interference between single resonant and non-resonant diagrams, give the last, non-resonant, contribution. For both reactions the four terms have been numerically integrated using Vegas [16] and the resulting distributions have been summed in the end.

The relative size of the different contributions is obviously dependent on the gauge and only the sum of all terms is gauge independent. In a given gauge however one can meaningfully discuss the numerical significance of the various expressions. In particular, in the physical, purely transverse gauge we have employed, there is a clear hierarchy between the four contributions in which we have divided the full cross section. The double resonant contribution is always much larger than the single resonant ones, which in turn dominate the non-resonant term.

We have verified numerically that in NWA the total cross sections calculated from the double resonant subsets reproduce the results obtained for $gg \to \bar{t}t$ and $q\bar{q} \to \bar{t}t$ for on shell top-quarks.

We have used the MRS(D_) [17] set of parton distribution functions throughout this paper. For α_s we have used the one-loop expression with $Q^2 = M_t^2$. A different choice of parton distribution functions or of the scale at which α_s is evaluated would slightly alter our results for the various cross section. However we are here mainly interested in the *relative* weight of the different contributions and their ratio is essentially insensitive to these choices.

3. Results

Our results for the total cross section are presented in Tables 1 and 2. For the Tevatron we have studied only the energy available at present, $\sqrt{s} = 1.8$ TeV, neglecting possible improvements that have been recently discussed in the literature. The LHC will probably begin its operation with a center of mass energy of 10 TeV which will be raised after a few years of running to $\sqrt{s} = 14$ TeV. Both energies have thus been ex-

Table 1
Tree level total cross sections in pb for $p\bar{p} \to b\bar{b}W^+W^-$ at $\sqrt{s} = 1.8$ TeV, $pp \to b\bar{b}W^+W^-$ at $\sqrt{s} = 10$ TeV and $pp \to b\bar{b}W^+W^-$ at $\sqrt{s} = 14$ TeV with $m_{\rm top} = 150, 175, 200$ GeV. The first and second column refer to the contribution of double resonant diagrams and to the contribution of single resonant diagrams and of the interference between single and double resonant diagrams in gluon-gluon fusion respectively. The third and fourth column report the contribution from double resonant production via $q\bar{q}$ fusion into a gluon and into γ and Z^0 bosons respectively. The last column gives the sum of the four contribution

		$m_{\rm top}$	gg $t\bar{t}$	gg bckgrd	$q\bar{q}$ $t\bar{t}$(strong)	$q\bar{q}$ $t\bar{t}$(el.weak)	total cross section
$p\bar{p}$	$\sqrt{s} = 1.8$ TeV	150 GeV	1.219	0.075	6.53	0.157	7.98
		175 GeV	0.340	0.036	3.07	0.076	3.52
		200 GeV	0.101	0.018	1.49	0.037	1.64
pp	$\sqrt{s} = 10$ TeV	150 GeV	418.	18.	63.2	1.40	500.
		175 GeV	201.	12.	35.3	0.79	249.
		200 GeV	104.	8.5	21.0	0.48	134.
pp	$\sqrt{s} = 14$ TeV	150 GeV	884.	38.	101.	2.2	1025.
		175 GeV	443.	26.	58.0	1.3	528.
		200 GeV	239.	19.	35.4	0.8	294.

Table 2
Tree level total cross section in pb and contribution in percentage of the most relevant channels to the total cross section for $pp \to b\bar{b}W^+W^-$ at $\sqrt{s} = 10$ TeV and at $\sqrt{s} = 14$ TeV with $m_{\rm top} = 150, 175, 200$ GeV. The first contribution arises from gluon fusion double resonant diagrams. The second one is the contribution from single resonant diagrams and from the interference between single and double resonant diagrams in the gluon fusion channel, while the third one derives from quark fusion double resonant diagrams. All other contributions are below 1% at tree level

		$m_{\rm top}$	total cross section	$gg \to b\bar{b}W^+W^-$ signal	$gg \to b\bar{b}W^+W^-$ background	$q\bar{q} \to b\bar{b}W^+W^-$ signal
pp	$\sqrt{s} = 10$ TeV	150 GeV	500. pb	83%	4%	13%
		175 GeV	249. pb	81%	5%	14%
		200 GeV	134. pb	78%	6%	16%
pp	$\sqrt{s} = 14$ TeV	150 GeV	1025. pb	86%	4%	10%
		175 GeV	528. pb	84%	5%	11%
		200 GeV	294. pb	82%	6%	12%

amined. For the top mass we have chosen three values which bracket the allowed range of variation, namely $M_t = 150$ GeV, $M_t = 175$ GeV and $M_t = 200$ GeV. In Table 1 we report the value of the total cross section, separating the contribution of the gg and $q\bar{q}$ channels. In the first case we further differentiate between the double resonant contribution, corresponding to the production of two nearly on-shell top quarks, and the background which is dominated by events in which only one top is produced close to its mass shell. In the $q\bar{q}$ channel we distinguish the standard mechanism in which the initial pair of light quarks annihilates to a gluon from the $\mathcal{O}(\alpha^4)$ contribution in which the $q\bar{q}$ pair annihilates to a photon or a Z boson. In both $q\bar{q}$-initiated processes all non-double resonant contributions are negligible. The rightmost column gives the sum of all partial results. All contributions not mentioned in Table 1 are negligible, well below the percent level.

Table 1 shows, as well known, that $q\bar{q}$ annihilation is the dominant source of $b\bar{b}W^+W^-$ events at the Tevatron, while the gg fusion channel contributes about 20% for $M_t = 150$ GeV and only about 7% for $M_t = 200$ GeV, due to the softer gluon spectrum at these energies. At the LHC this pattern is reversed, the gluon fusion mechanism provides the bulk of all events while the $q\bar{q}$ channel contributes between 10 and 20% depending on the top mass. We notice that

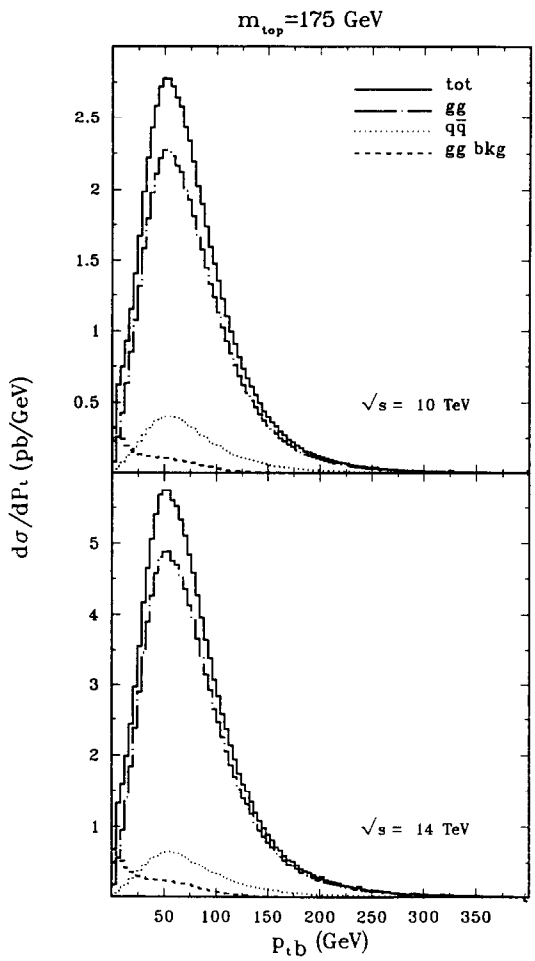

Fig. 3. The distribution of transverse momentum of the b quark for $pp \to b\bar{b}W^+W^-$ with $m_{\rm top} = 175$ GeV at $\sqrt{s} = 10$ TeV (a) and $\sqrt{s} = 14$ TeV (b). The dotted line represents the contribution from double resonant diagrams in the quark fusion channel, while the dash-dotted line is the contribution from double resonant diagrams in gluon fusion. The dashed line is the "irreducible background" from single resonant diagrams and from the interference between single and double resonant diagrams in the gluon fusion channel. The continuous line is the sum of the three contributions.

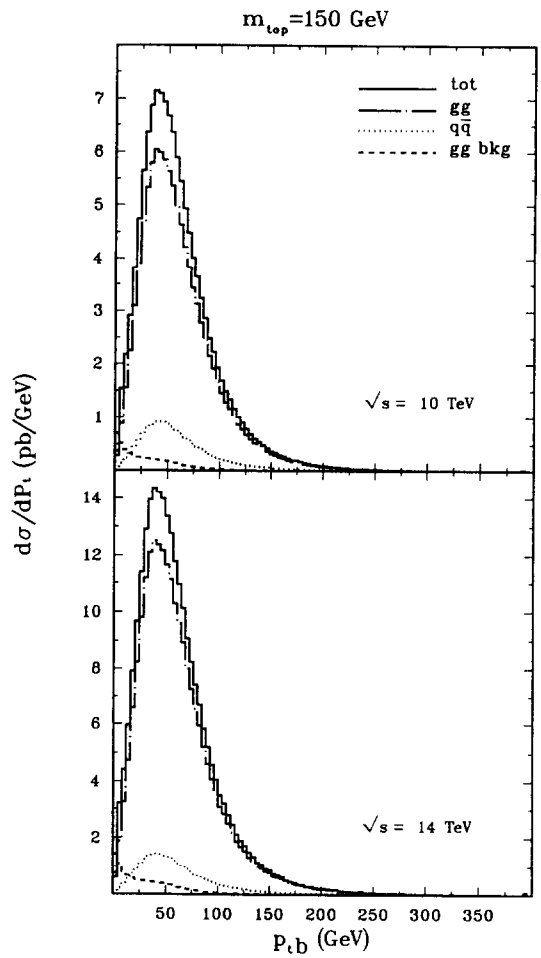

Fig. 4. The distribution of transverse momentum of the b quark for $pp \to b\bar{b}W^+W^-$ with $m_{\rm top} = 150$ GeV at $\sqrt{s} = 10$ TeV (a) and $\sqrt{s} = 14$ TeV (b). Symbols as in Fig. 3.

the $\mathcal{O}(\alpha^4)$ $q\bar{q}$ annihilation cross section is about 2.5% of the corresponding $\mathcal{O}(\alpha_s^2\alpha^2)$ results, independently of the top mass and of the collider energy. The gluon fusion background gives an important contribution to the cross section for $gg \to b\bar{b}W^+W^-$ at the Tevatron, between 6% for $M_t = 150$ GeV and 18% for $M_t = 200$ GeV. However it only contributes about 1% to the total cross section for $t\bar{t}$ production. At the LHC the gg background is smaller compared to the gg signal than at the Tevatron, but its contribution to the total $t\bar{t}$ cross section is larger. This can be appreciated in Table 2 where we present the contribution in percent to the total cross section at the LHC of the three main subprocesses, the double resonant channel $gg \to t\bar{t} \to b\bar{b}W^+W^-$, the single resonant channel $gg \to t\bar{b}W^-, \bar{t}bW^+ \to b\bar{b}W^+W^-$ and the double resonant $q\bar{q}$ contribution $q\bar{q} \to t\bar{t} \to b\bar{b}W^+W^-$, for the two energy values and the three values of the top mass which we have studied. The gluon fusion background contributes between 4% and 6% of the total gg cross section, the largest contribution being for the heaviest top mass. Comparing the second and third column in Table 2 we see that the gg background cross section is

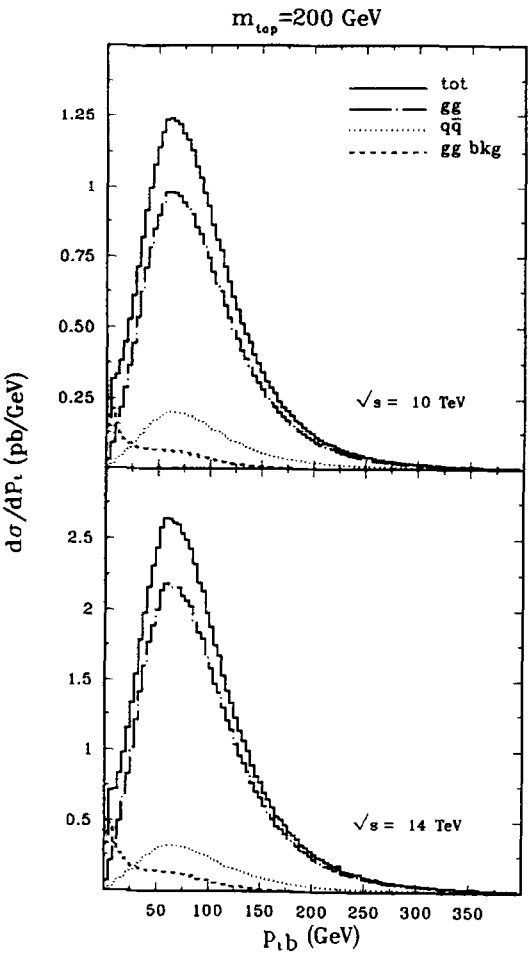

Fig. 5. The distribution of transverse momentum of the b quark for $pp \to b\bar{b}W^+W^-$ with $m_{top} = 200$ GeV at $\sqrt{s} = 10$ TeV (a) and $\sqrt{s} = 14$ TeV (b). Symbols as in Fig. 3.

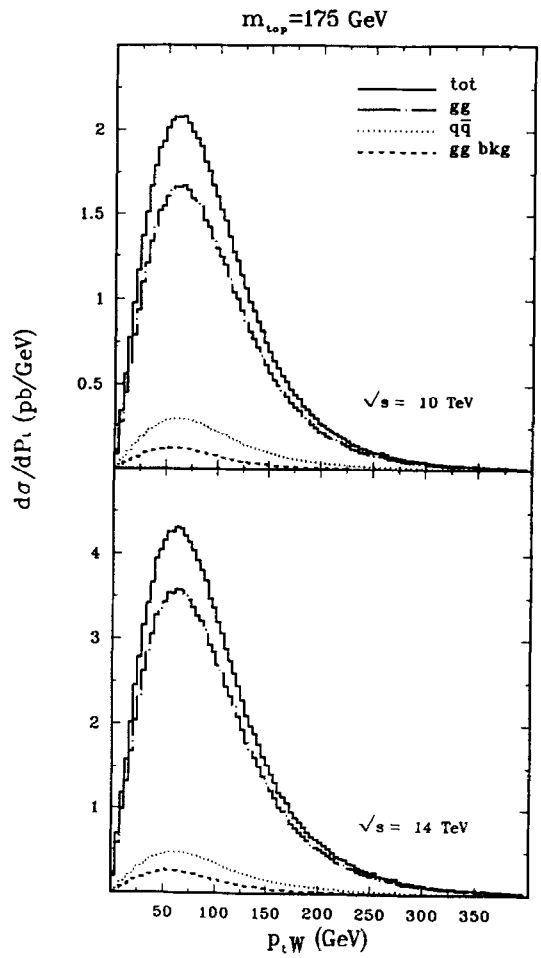

Fig. 6. The distribution of transverse momentum of the W^+ for $pp \to b\bar{b}W^+W^-$ with $m_{top} = 175$ GeV at $\sqrt{s} = 10$ TeV (a) and $\sqrt{s} = 14$ TeV (b). Symbols as in Fig. 3.

about one half of the total $q\bar{q}$ annihilation cross section.

In Figs. 3, 4 and 5 we present the transverse momentum distribution of the b-quark for $M_t = 175$, 150 and 200 GeV, respectively, at $\sqrt{s} = 10$ and 14 TeV. In Fig. 6 one can find the transverse momentum distribution of the W^+ for $M_t = 175$ GeV at both LHC energies. The two double resonant contributions and the gluon-gluon fusion background are shown separately and the full line gives the sum of the three distributions. Within the statistical errors of our Monte Carlo the distributions of the two double resonant channels differ only in overall normalization and have the same shape. The gg background p_T^b spectrum is peaked at small transverse momenta and shows a small hump at about 50 GeV. This can be easily understood noticing that this channel is dominated by diagrams, for instance diagram 6 and 7 in Fig. 1, in which the two initial state gluons split into $b\bar{b}$ pairs, producing b's with small p_T. A b from one pair and a $\bar{b}$ from the other then further interact annihilating to a W^+W^- pair through the exchange of a t-channel top. The large mass of the top prevents any substantial enhancement for small angle scattering and indeed the background p_T^W spectrum does not show any preference for small transverse momenta. It is however softer than the corresponding double resonant distribution, as can be seen if the different contributions are scaled to a common

height, say, of the maximum. The hump at large p_T^b is due to the presence of a single top in most of the background events.

A more refined analysis of the influence of backgrounds on $t\bar{t}$ production would require the introduction of a realistic set of experimental cuts. However, as already mentioned, the vast majority of background events contain one nearly on shell t-quark and they would survive most selection procedures optimized for the observation of top, leaving the signal to background ratio practically unchanged. A possible catch in the preceding argument has to do with the fact that the b-quark which is not produced in the decay of a top, has a soft p_T spectrum and some of the tracks from its own decay might miss the vertex detector, which is the most effective tool for b-tagging, whose geometrical coverage is limited. This might reduce the b-tagging efficiency for this channel in comparison with the double resonant one where both b's are equally hard. It is however extremely difficult to estimate this effect without a detailed simulation of b hadronization and of the full detector.

4. Conclusions

We have produced the complete matrix elements for $gg, q\bar{q} \to b\bar{b}W^+W^-$. With them we have analyzed $t\bar{t}$ production at the Tevatron and the LHC. With our approach we avoid separating the production process from the subsequent decay. Finite width effects, irreducible backgrounds and correlations between the two t-quark decays are included in our treatment.

We found that contributions from irreducible backgrounds provide about 1% of the total $t\bar{t}$ cross section at the Tevatron and become more relevant at the LHC, where they amount to about 5% of the total production rate. The reason for this difference is that single resonant channels are important for the gg cross section and not for the $q\bar{q}$ processes. The the $\mathcal{O}(\alpha^4)$ $q\bar{q}$ annihilation cross section is about 2.5% of the total at the Tevatron and is negligible at the LHC.

References

[1] F. Abe et al. (CFD Collaboration), Phys. Rev. 74 (1995) 2626;
S. Abachi et al. (D0 Collaboration), Phys. Rev. 74 (1995) 2632.
[2] G.F. Tartarelli for the CDF Collaboration, CDF/PUB/TOP/PUBLIC/3664.
[3] The LEP Coll. ALEPH, DELPHI, L3, OPAL and the LEP Electroweak Working Group, CERN-PPE/95-172, Nov. 1995.
[4] R.K. Ellis, Phys. Lett. B 259 (1991) 492.
[5] E. Laenen, J. Smith and W.L. van Neerven, Phys. Lett. B 321 (1994) 254;
E. Berger and H. Contopanagos, Phys. Lett. B 361 (1995) 115; hep-ph/9603326 (1996);
S. Catani, M. Mangano, P. Nason and L. Trentadue, hep-ph/9602208 (1996).
[6] N. Kidonakis and J. Smith, Phys. Rev. D 51 (1995) 6092.
[7] S. Frixione, M. Mangano, P. Nason and G. Ridolfi, Phys. Lett. B 351 (1995) 555.
[8] T. Stelzer and S. Willenbrock, hep-ph/9505433.
[9] R. Kleiss and W.J. Stirling, Z. Phys. C 40 (1988) 419.
[10] A. Ballestrero, E. Maina and S. Moretti Phys. Lett. B 333 (1994) 434.
[11] K. Hagiwara and D. Zeppenfeld, Nucl. Phys. B 274 (1986) 1.
[12] A. Ballestrero and E. Maina, Phys. Lett. B 350 (1995) 225.
[13] A. Ballestrero, in preparation.
[14] G.J. Gounaris, R. Kogerler and H. Neufeld, Phys. Rev. D 34 (1986) 3257.
[15] A. Ballestrero, E. Maina amd S. Moretti, Phys. Lett. B 335 (1994) 460.
[16] G.P. Lepage, J. Comp. Phys., 27 (1978) 192.
[17] A.D. Martin, W.J. Stirling and R.G. Roberts, Phys. Rev. D 50 (1994) 6734.